-RESEARCH PAPER-

International Journal of Mining and Geo-Engineering

IJMGE

IJMGE 60-2 (2026) 187-196

DOI: 10.22059/IJMGE.2026.382402.595196

Influence of blast geometry in the prediction of blast-induced vibration: a case study of granite aggregate quarries

Shaib Abdulazeez Shehu [a,b,*], Mohd Hazizan Mohd Hashim [b], Hareyani Zabidi [b], Michael Adebola Jethro [a], Kudirat Oziohu Yusuf [c] and Abdullateef Onimisi Jimoh [d]

[a] *Department of Civil and Mining Engineering, Confluence University of Science and Technology (CUSTECH), Osara 264103, Kogi State, Nigeria.*

[b] *School of Materials and Mineral Resources Engineering, University Sains Malaysia, Engineering Campus, Nibong Tebal, Malaysia.*

[c] *Department of Civil Engineering, Kogi State Polytechnic, Lokoja 260102, Nigeria.*

[d] *Department of Geology, Federal University, Lokoja 260102, Nigeria.*

Article History:

Received: 16 September 2024.
Revised: 23 November 2025.
Accepted: 03 May 2026.

ABSTRACT

Ground vibration is an inherent hazard of rock blasting and can impair the safety of lives and properties. Therefore, accurate prediction of vibration is imperative. Vibration is commonly evaluated using scaled distance without considering blast geometry. This study investigated the influence of blast geometry on the prediction of blast-induced vibration by using datasets from two quarries. Blast geometry was incorporated into the traditional scaled distance model to predict peak particle velocity (PPV). PPV was predicted by performing regression analyses using scaled distance and blast geometry as independent variables. Furthermore, the evaluated trend, sensitivity, and associated errors compared the predicted PPV with the measured PPV. The blast geometry modified approach in a nonlinear multiple regression model ranked best with an overall average grading of 90% and 92% on Excel Solver and SPSS iterations, respectively. Scaled distance is still the most potent factor in predicting blast vibration but yields lower accuracy when used without blast geometry. The cumulative performance of the investigated parameters using a neural network shows an excellent relationship between the predicted and measured peak particle velocities with a correlation coefficient of 0.93. Therefore, the traditional scaled distance should be complemented with blast geometry for better accuracy.

Keywords: *Blasting; Vibration; Peak particle velocity; Scaled distance; Blast geometry.*

1. Introduction

Blasting is the most common and cheapest rock excavation technique in mining and civil engineering practices. However, using explosives for rock blasting is associated with many human, structural, and environmental hazards [1, 2] because explosive energy is not one hundred percent efficient. Only 5 to 20% of the total explosive energy released during blasting is effectively used to achieve rock fragmentation [3, 4]. The effective energy used for rock breakage is in the form of shock and gas energy. The remaining surplus energy in the form of seismic, heat, light, and sound [5] causes various environmental and structural discomforts [1, 6]. This waste energy gives rise to ground vibrations, air overpressure (noise), and flyrock. Additionally, backbreak, overbreak, blast fumes, and changes in the natural profile of the ground are also part of the destructive effects of unexploited energy. These adverse effects of blasting are unavoidable and cannot be eliminated but can be mitigated to permissible levels to avoid human and environmental discomforts. Therefore, adequate control measures are necessary to minimize the potential danger of blast disturbances resulting from unutilized explosives.

Among the negative impacts of rock excavation by blasting, practicing engineers and government regulatory authorities give topmost priority to ground vibration. Therefore, accurate prediction and evaluation are vital to minimize its potential risk. The peak particle velocity (PPV) is the most reliable predictor for ground vibrations caused by blasting [7]. PPV has always been the basis of regulation and an essential indicator for evaluating ground vibrations since it can easily be estimated [8]. The most typical approach for quantifying blast-induced vibration using the concept of PPV has been the use of scaled distance (SD) as a predictor variable. Peak particle velocity generally increases with the maximum charge per delay. However, the work of Blair [9] studied the relationship between vibration waves from a single blasthole and that of a full-scale blast and observed that the traditional scaled distance approach to predict the peak velocity is associated with some problems. It was stated that vibration amplitudes could be reduced by applying suitable delays between blastholes without necessarily reducing charge weights. Previous researchers have proved that simulations can also be sued to improve the prediction of blast-induced ground vibration in rocks [10, 11] and concrete-like structures [12]. Therefore, safety and sustainability can be enhanced if alternate methods other than the traditional scaled distance approach are used to predict and simulate vibration [11].

Blair [9] analyzed large sets of vibration data from both underground and surface blasts and found that the PPV measured in underground blasting does not only depend on the charge weight. The works of various other researchers have equally proved that several other factors

* Corresponding author. *E-mail address:* shehuthefirst@yahoo.com (S.A. Shehu).

affect blast-induced vibration besides scaled distance and site constants [8, 13–16]. Dinlarloo [16] predicted blast vibration using the support vector machine in a large surface mine and observed that the burden is a significant factor in estimating peak particle velocity in production blasting. Faradonbeh and Monjezi [17] predicted vibration in an iron ore mine using gene expression programming (GEP). They observed that stemming and hole diameter significantly influence blast-induced ground vibration. Various studies have proved that incorporating other blast design parameters can enhance the traditional method of predicting peak particle velocity in mines and quarries [8, 18–24]. Thus, blast performance indicators can adequately predict blast loading, safety, and damage.

From the preceding, the prediction of blast-induced ground vibration using only the scaled distance approach is too conservative and may lead to difficulties in operating a quarry or mine efficiently and safely [25]. However, the scaled distance approach to vibration prediction is still very reliable but needs to be complemented for higher and better accuracy. This study examines the influence of blast geometry on blast-induced vibration in two granite aggregate quarries in Bukit Mertajam, Penang, Malaysia. The traditional scaled distance was complemented with a new concept of blast geometry (dimensions) to predict peak particle velocity.

2. Brief Description of Blast Geometry

Blast geometry is the configuration of a blast design defined by the burden (B), spacing (S), stemming length (SL), bench height (BH), charged length (LT), hole diameter (D), and subdrill (SD). The burden is the shortest perpendicular distance from the center of the blasthole to the available nearest free space. The burden is technically the distance between two rows of blastholes. The distance between adjacent blastholes within a row is called spacing.

Stemming length is the upper portion of the blasthole filled with inert materials such as drill cuttings and gravel to prevent gas venting. The vertical distance between the floor of a bench and its top level is called bench height. The blast hole diameter is defined and dictated by the bit diameter. Charged length (LT) is a summation of the column charge length and the stemming length. The stiffness ratio is the ratio of bench height to burden. Figure 1 defines blast geometry in a production bench blasting.

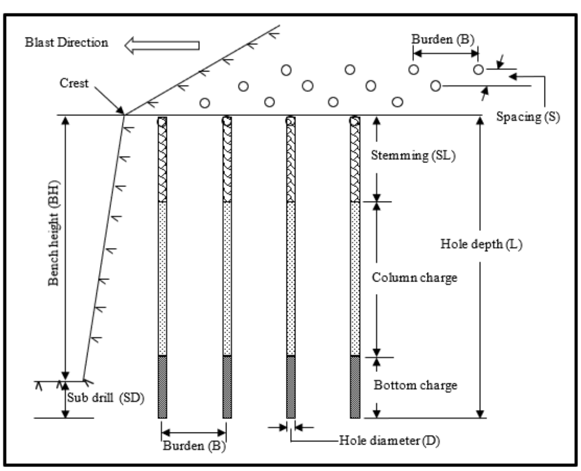

Figure 1. Illustration of blast geometry.

3. Importance of Blast Geometry Parameters and their Ratios

The most critical and essential dimension in blasting is the burden, and the choice of a burden will affect the entire blast performance [26]. The burden ratio can help determine the most appropriate burden compared to the hole or explosive diameter [27]. Too small or too big a burden will affect the blast performance negatively [26].

Previous investigations about the mechanism of rock fragmentation have observed that the most significant ratio in rock blasting is the spacing to burden (S:D). The term "stiffness ratio" (BH : B) equals the bench height divided by the Burden. The stiffness ratio must be chosen to conform with the hole diameter (D) for the best blast performance. Konya [28] recommended that the stiffness ratio should be between 2 and 4. It was argued that too much stiffness ratio could cause excessive vibration and flyrock. For effective blast results, the burden and the depth of the drillhole must be reasonably compatible. Generally, the drillhole depth-to-burden ratio should be between 1.4 and 4.0 [29]. A hole depth smaller than 1.5 times the burden causes excessive vibration, air blast, flyrocks, and uneven fragmentation [29].

The stemming length is commonly evaluated relative to the hole depth and diameter. Stemming effectively utilizes explosive energy and allows the distribution of the energy in the blast hole [30]. Inappropriate stemming can lead to early escape of detonation gasses in advance and result in waste of explosive energy, poor fragmentation, and various environmental problems, such as ground vibration, flyrock, airblast, backbreak, overbreak, etc. [31].

Key geometric ratios in blasting that control blast outcomes and vibration are:

Burden (B) to Spacing (S): The relationship between these two parameters (the S/B ratio) is critical for efficient fragmentation and controlling the maximum charge per delay. A well-designed S/B ratio ensures uniform rock breakage, reducing the need for excessive charge, which in turn minimizes vibration [30, 32].

Stemming Length (SL) to Burden (B): This ratio is essential for confinement, directly controlling the effective energy applied to the rock and limiting the immediate-source contribution to ground vibration [30].

Bench Height (BH) to Burden (B): This ratio, known as the Burden Stiffness Ratio (typically 2 to 4 for good fragmentation), relates the bench's structural scale to the burden. An appropriate stiffness ratio is generally a measure of blast quality and efficiency, , which, in turn, indirectly affects the required charge and, thus, vibration [29].

Burden (B) to Hole Diameter (D): The (B/D) ratio primarily determines the degree of rock confinement relative to the size of the explosive column. A larger hole diameter allows for a larger charge, requiring a correspondingly larger burden to contain the explosive force effectively. This ensures that the explosive energy is used for breaking the rock mass rather than escaping too easily. An optimal range (typically 25-35) balances efficient rock fragmentation while minimizing the maximum charge needed, thus controlling blasting vibration (PPV) [26].

Charge Length (L) to Hole Diameter Ratio (D): The L/D ratio represents the geometry of charge distribution. It affects the frequency and amplitude of ground vibrations. Long charge columns (high L/D) tend to produce low-frequency vibrations capable of travelling longer distances with minimal attenuation [33]. Decoupled charges, where the charge diameter is smaller than the borehole diameter, significantly reduce PPV due to reduced coupling efficiency. Proper selection of charge geometry contributes to improved fragmentation and reduced vibration levels [34].

From the above discussions on the importance of the blast dimensions and their ratios, one can infer that some of the most vital proportions of blast geometry in rock blasting using explosives are S : B, B:D, BH : B, and LT : SL. Thus, the influence of these ratios on blast-induced ground vibration was investigated in this study.

4. Effects of Blast Geometry on Vibration

The effect of blast geometry on vibration attenuation has been least understood and therefore deserves attention. The charge diameter of bulk explosives is nominally equal to the diameter of blastholes. Adequate consideration has not been given to the effects of hole diameter because mining or construction companies rarely change their drill bits. Usually, only one type of drill bit is sufficient for a company. Drill bits are typically chosen to maximize productivity without the interest of changing the hole diameter. The velocity of detonation (VOD) increases with the blast hole diameter [35]. Smaller blastholes can reduce the performance of explosives to the point of critical diameter where the explosives may fail to detonate [36]. Blast holes of larger diameters tend to cause more vibration than smaller ones.

Peak particle velocity significantly depends on charge diameter and not solely charge weight because the charge density is a function of hole diameter [8, 9, 37, 38]. An increase in hole diameter allows explosives to detonate at a higher velocity. This increased velocity leads to higher explosive energy and, consequently, a higher vibration level. A reduction in the drill hole diameter without a proportionate change in burden and spacing lowers the powder factor and yields low vibration but coarser fragmentation [39].

Vibrations in longer blastholes produce higher peak particle velocities at lower frequencies than in short holes since vibration amplitudes are very sensitive to the volume of shock waves [8, 9]. The volume of the shock wave depends on the diameter and depth of the blasthole.

Blasting occurs within the rock mass and does not reach the surface. The inside of a rock mass exhibits different failures with varying distances of burden. Uysal et al. [40] studied blast vibrations for different widths of burdens ranging from 3 to 14 m. They affirmed that burden width significantly impacts vibrations, and that insufficient burden will lead to higher vibration levels by creating more waste energy due to the large volume of venting gasses. Accordingly, vibration increases as the burden decreases [24, 41].

Hole depth is usually altered based on blasting conditions. In a relatively large hole depth, most of the explosive energy is dissipated within the rock mass, causing little vibration. In a relatively small hole depth, a large proportion of explosive energy causes higher vibration, over breaks, and flyrock. Therefore, hole depth has an optimal range based on its effect on blast-induced ground vibration.

Stemming is an area with no column charge and significantly impacts vibration. An area with no explosive implies that vibration would ordinarily be meager in this region. Disproportionately smaller stemming columns to hole diameter usually cause vibration [13], airblast, flyrock, and overbreaks. Some researchers [39, 42] believed that a long stemming length is the best for a highly weathered rock with several joint sets. For competent massive rock, the stemming column is mostly kept short. The general trend is that the peak particle velocity increases with an inappropriate ratio of stemming length to burden.

Various investigations have shown that PPV varies with stemming, hole depth, and spacing in different and ambiguous ways. The common conclusion is that the PPV is maximum if the hole depth, stemming length, and spacing are below specific critical values [8, 17, 43, 44]. Thus, inadequate depth, stemming, and spacing can result in unnecessary higher vibrations.

5. Materials and Methods

Datasets were obtained from two granite aggregate quarries and randomly classified into regression and testing data. Regression analyses were carried out using multiple linear regression and the traditional USBM (US Bureau of Mines) model. The usual USBM model was evaluated with the recommended and specifically calculated site constants. Ratios of some blast geometry parameters were further used to modify the traditional USBM model in a nonlinear multiple regression format. The attenuation constants of the newly revised nonlinear USBM model were evaluated using the Excel Solver's generalized reduced gradient (GRG) algorithm and the Levenberg-Marquardt algorithm of SPSS. The Predicted PPVs were compared with measured PPVs using statistical error and sensitivity analyses. The tested models were then graded based on the error analyses. Additionally, the importance of the regression parameters was evaluated using the multilayer perceptron algorithm of the neural network.

5.1. Description of the Study Quarries

FYS and Kuad quarries are located in Berapit and Penanti, respectively, within the metropolis of Bukit Mertajam in Sebarang Perai Tengah District, Peninsula Malaysia. Figure 2 shows the location of the study sites. The top left of Figure 2 shows the state of Pulau Pinang in Peninsula Malaysia, while the down left shows the Seberang Perai Tengah District in Pulau Pinang. The larger right side shows the location of the study quarries in Seberang Perai District and the most popular bust stop in Bukit Mertajam (The Summit Hotel).

Berapit has a longitude of 100°28'51.69" E and a latitude of 05°23'9.16" N. The closest residential area is about 334 m away from the FYS quarry. Penanti is of longitude 100°28'59.99" E and latitude 05°23'59.99" N. Kuad quarry is about 655 m from the closets residential area. The two quarries produce granite aggregates for the construction industry in Malaysia.

Bukit Mertajam is the administrative headquarters of Seberang Perai in Penang, Malaysia. It is located close to Mertajam Hill and encircled by flat alluvial plains [45]. Bukit Mertajam borders Permatang Pauh to the north, Permatang Tinggi and Alma to the south, Mengkuang Titi to the east, and Bukit Tengah to the west.

The Bukit Mertajam Kulim (BMK) granite is a lonely body positioned within northwest Peninsular Malaysia. The granite lies west of the Bintang batholith and forms part of the Western Belt granite of Peninsular Malaysia. The Penang granite lies west of BMK granite, which makes up the entire Penang Island [46]. The BMK granite comprises three core units, the Mertajam, the Bongsu, and the Panchor granites, which were deposited reasonably short time between 180 to 224 Ma. All three units contain fine to coarse-grained porphyritic rocks [46].

5.2. Description of the Research Data

Sixty-seven (67) blast data from the two studied quarries were used to study the effects of blast geometry on vibration. Of these datasets, thirty-six (36) were from the FYS quarry, and thirty-one (31) were from the Kuad quarry. The entire data were grouped randomly into two, the regression data and the testing data. The regression data consists of 52 blast events, while testing data has 15 blast events. The data collected for each blast event are the burden (B), spacing (S), stemming length (SL), hole depth (L), charge length (LT), bench height (BH), hole diameter (D), scaled distance (SD), and the peak particle velocity (PPV). Tables 1 and 2 describe the basic statistics of the regression and testing data, respectively.

In this study, the PPV was taken as a dependent variable and was predicted using SD and the ratios of blast geometry parameters (S:B, B:D, BH:B, and LT:SL) as independent variables.

5.3. Multiple Linear Regression (MLR)

Multiple linear regression (MLR) establishes a linear relationship between an output parameter (dependent variable) and two or more input parameters (independent variables). The principle is centred on minimizing the sum of squares of disparity between the output and input parameters. The generalized form of multiple linear regression is shown in Equation 1.

$$Y = \beta_0 + \beta_1 X_1 + \beta_2 X_2 + \beta_3 X_3 + \cdots + \beta_n X_n + \varepsilon \tag{1}$$

where Y is the output parameter (dependent variable); $X_1, X_2, X_3, \ldots X_n$ are the inputs (independent variables); β_1, β_2, β_3, ... β_n are the coefficients of the input parameters; β_0 is the intercept, and ε is the sum of associated random errors.

Multiple linear regression is one of the most common approaches for establishing relationships between variables in sciences, management, and engineering. Multiple linear regression has been used by many [37, 47–49] to predict blast-induced vibration in mines and quarries. Hence, the model was one of the tested approaches in this study. The peak particle velocity was predicted from the scaled distance (SD) and ratios of blast geometry parameters in accordance with Equation 2.

$$PPV = I + \beta(SD) + a\left(\frac{S}{B}\right) + b\left(\frac{B}{D}\right) + c\left(\frac{BH}{B}\right) + d\left(\frac{LT}{SL}\right) \tag{2}$$

where I is the intercept, and β, a, b, c, and d are coefficients of the independent variables.

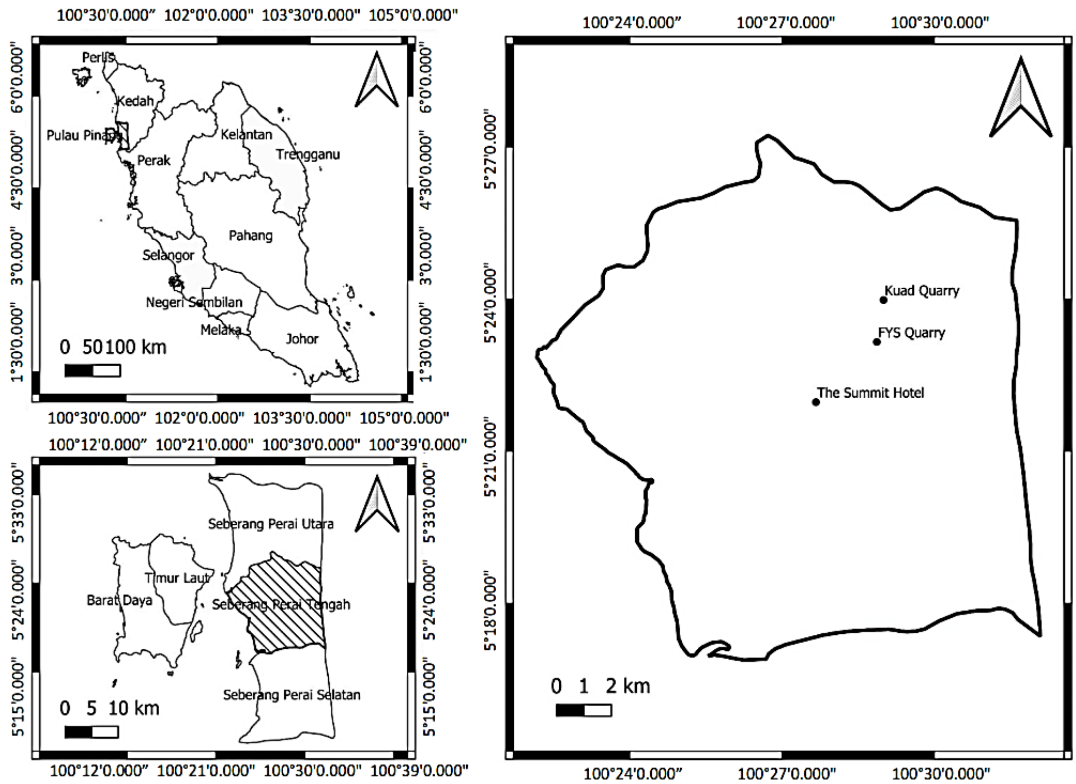

Figure 2. Location of the study quarries.

Table 1. Basic descriptive statistics of regression data.

Parameter	Unit	Symbol	Category	Min.	Max.	Mean	Std.
Scaled distance	m $kg^{-1/2}$	SD	Independent	61.02	132.56	94.96	22.40
Burden	m	B	Independent	2.44	3.96	2.98	0.47
Spacing	m	S	Independent	3.05	4.88	4.04	0.81
Hole diameter	m	D	Independent	0.089	0.089	0.089	0.00
Hole depth	m	L	Independent	6.10	13.11	11.36	1.93
Stemming length	m	SL	Independent	2.44	3.66	2.94	0.52
Bench height	m	BH	Independent	5.80	12.20	10.87	1.75
Charge length	m	LT	Independent	2.44	10.67	8.42	2.34
Peak particle velocity	mm/s	PPV	Dependent	0.50	2.43	1.22	0.47

Table 2. Basic descriptive statistics of testing data.

Parameter	Unit	Symbol	Category	Min.	Max.	Mean	Std.
Scaled distance	m $kg^{-1/2}$	SD	Independent	68.98	130.63	95.24	18.34
Burden	m	B	Independent	2.44	3.96	2.95	0.38
Spacing	m	S	Independent	3.05	4.88	4.07	0.79
Hole diameter	m	D	Independent	0.089	0.089	0.089	0.000
Hole depth	m	L	Independent	6.10	13.11	11.32	2.12
Stemming length	m	SL	Independent	2.44	3.66	3.01	0.57
Bench height	m	BH	Independent	5.80	12.20	10.73	1.91
Charge length	m	LT	Independent	2.44	10.67	8.35	2.61
Peak particle velocity	mm/s	PPV	Dependent	0.62	1.73	1.18	0.35

5.4. USBM Predictor Using Recommended Site Constants (USBM RM)

Peak particle velocity has been consistently predicted using scaled distance (SD) [50–54]. The most reliable relationship between blast geometry and ground vibration relates particle velocity to scaled distance. The square root scaled distance (SD) is defined as shown in Equation 3:

$$SD = \frac{R}{\sqrt{W}} \tag{3}$$

where:

W = The maximum instantaneous charge (MIC) (kg).

R = The radial distance from the detonation point to the observation point (m).

The maximum instantaneous charge is the maximum amount of explosive detonated per delay. The peak particle velocity was predicted using the scaled distance equation developed by the United State Bureau of Mines (USBM) [55–57], as shown in Equation 4.

$$PPV = k(SD)^{\beta} = k\left(\frac{R}{\sqrt{W}}\right)^{\beta} \tag{4}$$

where:

PPV = Peak particle velocity (mm/s).

k, β = Site constants that are related to rock factors.

The Standards Association of Australia [58] recommended the values of k and β as 1140 and −1.6, respectively, for the studied rock type having a free face for rock displacement under normal confinement. These recommended constants translate Equation 4 to Equation 5.

$$PPV = 1140(SD)^{-1.6} = 1140\left(\frac{R}{\sqrt{W}}\right)^{-1.6} \tag{5}$$

5.5. USBM Predictor Using Evaluated Site Constants (USBM EV)

Researchers have argued that the attenuation constants used to predict blast-induced vibration in the USBM model are site specifics [59–61] and vary with the geological and strength characteristics of formations. To this end, the site constants k and β of Equation 4 were evaluated using the regression data. Taking the log of both sides, Equation 4 transforms to 6.

$$\log_{10} PPV = \beta \times \log_{10} SD + \log_{10} k \tag{6}$$

The values of $\log_{10} PPV$ was plotted against $\log_{10} SD$ to obtain the constants k and β.

5.6. Nonlinear Multiple Regression Using Excel Solver (NMR SV)

Nonlinear multiple regression is the modelling of observational data by a nonlinear combination function of two or more independent variables (inputs) to predict one dependent variable (output). A process of successive iterations fits the observational data. Any model that is not linear in form can be described as nonlinear. Nonlinear regression fits data to a specified model. Equation 7 represents the general form of a nonlinear model.

$$Y = f(X, \beta) + \varepsilon \tag{7}$$

where Y is the dependent variable (output), X is a vector of p predictors, β is a vector of k parameters, f(·) is a known regression function, and ε is an error term. The error term may or may not be normally distributed.

The nonlinear model is very versatile due to its flexibility to fit various curves. Nonlinear regression has been used to predict vibrations in mining and civil engineering projects [17, 62]. The nonlinear regression model may be quadratic, power, exponential, inverse, polynomial, or logarithmic.

This study utilized a nonlinear function of the form displayed in Equation (8) to evaluate the regression data using the Excel Solver by the minimization method. The Excel Solver's generalized reduced gradient (GRG) nonlinear algorithm was adopted.

$$PPV = k(SD)^{\beta} \times \left(\frac{S}{B}\right)^{a} \times \left(\frac{B}{D}\right)^{b} \times \left(\frac{BH}{B}\right)^{c} \times \left(\frac{LT}{SL}\right)^{d} \tag{8}$$

where k and β are the initial specific site constants evaluated from the USBM prediction method; constants a, b, c, and d assumed initial values of 0. The possible optimal values of k, β, a, b, c, and d were evaluated by setting the sum of square errors of PPV predicted from Equation 8 as the objective function and the initial values of k, β, a, b, c, and d as the changing variables. The sum of square errors was calculated using Equation 9.

$$\sum_{i=1}^{n}\left(\frac{PPV_{meas} - PPV_{pred}}{PPV_{meas}}\right)^{2} \tag{9}$$

where PPV_{meas} is the measured value of PPV; PPV_{pred} is the predicted value of PPV, and n is the number of regression data used.

5.7. Nonlinear Multiple Regression Using SPSS (NMR SP)

Equation 8 was further solved using IBM SPSS Statistics software, Campus Edition V24.0, owned by the Universiti Sains Malaysia, Engineering Campus, Nibong Tebal, using the inbuilt Levenberg-Marquardt algorithm. PPV was set as a dependent variable while SD, S/B, B/D, BH/B and LT/SL are independent variables. The constants k, β, a, b, c, and d were taken as parameters to be determined with the same initial values as assigned in the Excel Solver solution.

5.8. Characteristics of the Regression Models

The five regression techniques used have inherent advantages and disadvantages. Table 3 summarises each method's characteristics, advantages, and disadvantages.

5.9. Performance Indicators of the Models

The predicted values of PPV from the models were compared with the actual measured values. A comparison was also made between the predicted PPV and the measured PPV by evaluating their trend, sensitivity, and associated errors. The determination coefficient (RSQ), the variance accounted for (VAF), mean absolute percentage error (MAPE), mean absolute error (MAE), and the root mean square error (RMSE) were the indicators used to analyze the predicted PPV.

RSQ (determination coefficient) is the square of the Pearson product-moment correlation coefficient through the given data points. It is called R-squared or coefficient of determination. RSQ represents the proportion of the dependent variable explained by the independent variable(s). It measures the fitness level of observed data by a regression model, and its value ranges from 0 to 1. A higher value of RSQ indicates a better fit. RSQ was evaluated for each model by using Equation 10.

$$RSQ = \frac{\sum_{i=1}^{n}\left(PPV_{pred} - \overline{PPV}_{mean}\right)^{2}}{\sum_{i=1}^{n}\left(PPV_{meas} - \overline{PPV}_{mean}\right)^{2}} \tag{10}$$

where n is the number of data; PPV_{pred} is the predicted value of PPV; $\overline{PPV}_{mean}$ is the mean of the measured PPV values; and PPV_{meas} is the measured PPV.

VAF (variance accounted for) is used to measure the precision of a model. It measures the correctness of a model by comparing the measured value with the predicted value. The value of VAF is 100% if the measured value is the same as the observed value [63]. If the two values differ, the VAF is lower. The higher the VAF value, the higher the precision of the predictive model [64]. Equation 11 was used to calculate VAF for each model.

$$VAF = \left[1 - \frac{var(PPV_{meas} - PPV_{pred})}{var(PPV_{meas})}\right] \tag{11}$$

where var represents the variance.

MAPE (mean absolute percentage error) is a statistical measure of the mean of the absolute percentage errors of predictions. It is the summation of absolute percentage errors divided by the number of data sets. Error is defined as the difference between the measured value and the predicted value. The lower the value of MAPE, the better the prediction model [65]. A MAPE value of 100% indicates that the model does not represent the data set. Dindarloo (2015) used MAPE to analyze predicted PPV values using the support vector machine, which was very effective. Equation 12 defines MAPE.

$$MAPE = \frac{1}{n}\sum_{i=1}^{n}\left|\frac{PPV_{meas} - PPV_{pred}}{PPV_{meas}}\right| \tag{12}$$

MAE (mean absolute error) is a loss function that evaluates the performance of a regression model. MAE measures the absolute differences between measured and predicted variables. It is basically the arithmetic average of the absolute errors in a set of predictions, as expressed in Equation 13. A higher value of MAE shows the poor quality of the predictive model.

$$MAE = \frac{1}{n}\sum_{i=1}^{n}\left|PPV_{meas} - PPV_{pred}\right| \tag{13}$$

Table 3. Characteristics, advantages, and disadvantages of the regression methods used.

Methods	Characteristics	Advantages	Disadvantages
Multiple Linear Regression (MLR)	Establishes a linear relationship between a dependent variable and two or more independent variables.	Unlimited number of independent variables. Very easy to implement, interpret and train.	Cannot fit complex datasets properly. It performs poorly when relationships are not truly linear.
USBM Predictor Using Recommended Site Constants (USBM RM)	The universal recommended site constants k and β are 1140 and −1.6, respectively	No need to evaluate site constants from a series of iterations. Good for preliminary assessments.	Universal site constants perform poorly because they do not obey the heterogenous nature of rocks.
USBM Predictor Using Evaluated Site Constants (USBM EV)	The site constants k and β are specifically evaluated from a series of blast data through iterations or simulations.	More precise than just adopting universal constants because it accounts for the heterogeneous nature of rocks.	Evaluation of specific site constants involves a series of iterations and is time-consuming.
Nonlinear Multiple Regression Using Excel Solver (NMR SV)	The initially evaluated site constants (k and β) are optimized by adopting the Excel Solver's generalized reduced gradient (GRG) nonlinear	The sum of square errors in the initially evaluated site constants is significantly minimized. The application is a free and flexible	The Excel Solver may stop before finding an optimal solution. Poor scaling affects solution time and quality. Non-convex objectives
Nonlinear Multiple Regression Using SPSS (NMR SP)	The initially estimated site constants (k and β) are enhanced by adopting the inbuilt Levenberg-Marquardt algorithm.	The associated errors in the initially evaluated site constants are minimized. It can handle both qualitative and quantitative data.	The application is not free. It cannot be used to analyze a very large data set. The graph features are not as simple as that of Microsoft Excel.

RMSE (root mean square error) is the square root of the average of squared residuals. It is the standard deviation of prediction errors. It measures prediction accuracy by comparing the forecasting errors of two or more models [66].The effect of each error on RMSE is proportional to the size of the squared error [67]. Hence, larger errors have an excessively more significant impact on RMSE. RMSE ranges from 0 to 1. RMSE value of 0 indicates a perfectly fit model of the dataset. The smaller the RMSE value, the better the model. Equation 14 was used to evaluate the RMSE of each of the models.

$$RMSE = \sqrt{\frac{1}{n}\sum_{i=1}^{n}\left(PPV_{meas} - PPV_{pred}\right)^2} \qquad (14)$$

5.10. Grading of the Models

The five models were ranked from 1 to 5 based on their levels of fitness of research data as defined by the five performance indicators. The best-fit model for an indicator was assigned a value of 5, while the poorest fitness was 1. Where a tie exists between two or more models, they were given the same rank, and the next lower rank is omitted. The final grading was calculated using Equation 15.

$$Model\ grade = \frac{1}{TR}\sum_{i=1}^{n}(Ranks) \times 100\% \qquad (15)$$

where TR is the total obtainable rank, which is 25, and n is the number of performance indicators, which is 5.

5.11. Performance of the Regression Parameters

The influence of the blast parameters on the predicted PPV of blast-induced vibration was further investigated by combining all the datasets. The entire data was analyzed using the multilayer perceptron algorithm of the neural network by making PPV the dependent variable and the other five parameters independent variables. The data set was partitioned into 80% training and 20% testing. The network architecture consists of a minimum layer of one and a maximum of 50. The maximum training time was set to 15 minutes.

6. Results and Discussion

The multiple linear regression of the datasets gives the intercept (I) of Equation 2 as 5.38 and the coefficients β, a, b, c, and d as -0.02, -0.84, -0.04 and 0.12, respectively. Substituting these values in Equation 2 gives Equation 16. Equation 16 further predicted the regression and testing data with determination coefficients of 0.88 and 0.93, respectively.

$$PPV = 5.38 - 0.02(SD) - 0.84\left(\frac{S}{B}\right) - 0.04\left(\frac{B}{D}\right) - 0.04\left(\frac{BH}{B}\right) + 0.12\left(\frac{LT}{SL}\right) \qquad (16)$$

The USBM model with the recommended attenuation constants k and β as 1140 and −1.6, respectively (Equation 4), gives resultant coefficients of determination of 0.78 on the regression data and 0.76 on the testing data.

To evaluate the specific site constants k and β, Figure 3 shows the graphical analysis between the log of the scaled distance (SD) and the log of the peak particle velocity (PPV) for the regression data as depicted in Equation 6. Both logs were taken to base 10 for easy interpretations, as suggested by Wyllie and Mah [68].

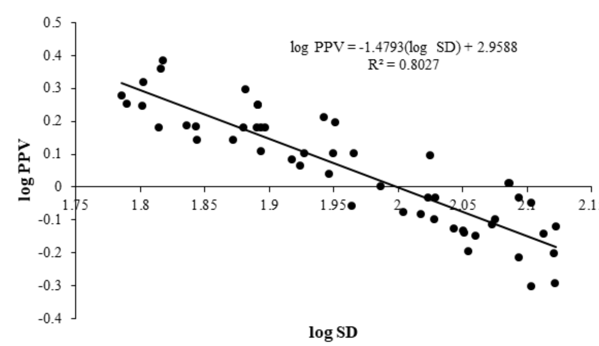

Figure 3. log–log plot of SD and PPV.

Equation 17 shows the established log-log relationship between the peak particle velocity (PPV) and the scaled distance (SD), with a strong determination coefficient of 0.80 for the regression data.

$$\log_{10} PPV = -1.4793 \log_{10} SD + 2.9588 \qquad (17)$$

In line with Equation 4, the associated attenuation site constants β and k for the regression data are −1.48 and 909.49 ($10^{2.9588}$), respectively. The slope of the line gives the constant β, while the intercept of PPV represents the value of k at a scaled distance of unity [68, 69]. Substituting these constants in Equation 4 gives Equation 18 for the regression data. Applications of Equation 18 on the regression and test data give determination coefficients of 0.79 and 0.77, respectively.

$$PPV = 909.49(SD)^{-1.48} = 909.49\left(\frac{R}{\sqrt{W}}\right)^{-1.48} \qquad (18)$$

Using these evaluated site constants k and β (909.49 and −1.48, respectively); and putting the initial values of constants a, b, c, and d as 0, the optimal values of k, β, a, b, c, and d obtained from the generalized reduced gradient (GRG) nonlinear algorithm of the Excel Solver as 225,303.95, −1.56, −1.00, −1.39, −0.28, and 0.33, respectively. By substituting these values in Equation 8, Equation 19 was obtained to predict the regression and testing data with determination coefficients of 0.94 and 0.93, respectively.

$$PPV = 225{,}303.95(SD)^{-1.56} \times \left(\frac{S}{B}\right)^{-1.00} \times \left(\frac{B}{D}\right)^{-1.39} \times \left(\frac{BH}{B}\right)^{-0.28} \times \left(\frac{LT}{SL}\right)^{0.33} \quad (19)$$

Similarly, the optimal values of constants k, β, a, b, c, and d were obtained from the Levenberg-Marquardt algorithm of SPSS as 1123894.48, −1.51, −0.88, −1.83, −0.59 and 0.44 respectively. Further substitution of these values in Equation 8 gave rise to Equation 20, which was used to predict the regression and test data with determination coefficients of 0.94 and 0.91, respectively.

$$PPV = 1{,}123{,}894.48(SD)^{-1.51} \times \left(\frac{S}{B}\right)^{-0.88} \times \left(\frac{B}{D}\right)^{-1.83} \times \left(\frac{BH}{B}\right)^{-0.59} \times \left(\frac{LT}{SL}\right)^{0.44} \quad (20)$$

Tables 4 and 5 compare the values of the performance indicators of the studied models for regression and testing data, respectively. Figure 4 illustrates the cumulative performance of each model on the datasets. Line graphs comparing the measured and predicted values of the PPVs for the regression and testing datasets are shown in Figures 5 and 6, respectively.

Table 4. Performance of the models based on the regression data.

Indicator	MLR:		USBM RM:		USBM EV:		NMR SV:		NMR SP:	
	Value	Rank	Value	Rank	Value	Rank	Value	Rank	Value	Rank
RSQ	0.88	3	0.78	1	0.79	2	0.94	4	0.95	5
VAF (%)	88.29	3	75.52	1	78.52	2	93.77	4	94.58	5
MAPE (%)	11.86	3	26.28	1	14.77	2	7.39	5	8.14	4
MAE	0.13	3	0.34	1	0.18	2	0.08	5	0.08	5
RMSE	0.16	3	0.41	1	0.22	2	0.12	4	0.11	5
Grade	60%		20%		40%		88%		96%	

Table 5. Performance of the models based on the testing data.

Indicator	MLR:		USBM RM:		USBM EV:		NMR SV:		NMR SP:	
	Value	Rank	Value	Rank	Value	Rank	Value	Rank	Value	Rank
RSQ	0.93	5	0.76	1	0.77	2	0.93	5	0.91	3
VAF (%)	90.14	3	71.32	1	75.83	2	92.76	5	90.16	4
MAPE (%)	8.69	3	27.99	1	11.19	2	5.98	4	5.63	5
MAE	0.09	3	0.34	1	0.13	2	0.08	4	0.07	5
RMSE	0.11	5	0.39	1	0.17	2	0.11	5	0.11	5
Grade	76%		20%		40%		92%		88%	

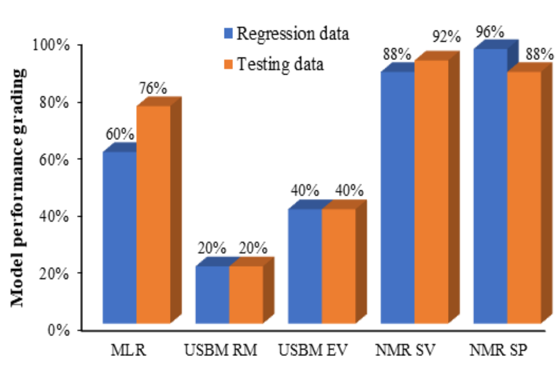

Figure 4. Cumulative performance of each model.

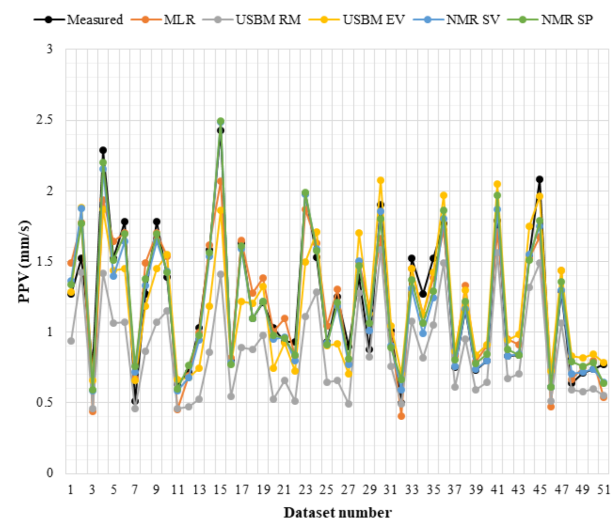

Figure 5. Comparison of measured and predicted PPVs of regression dataset.

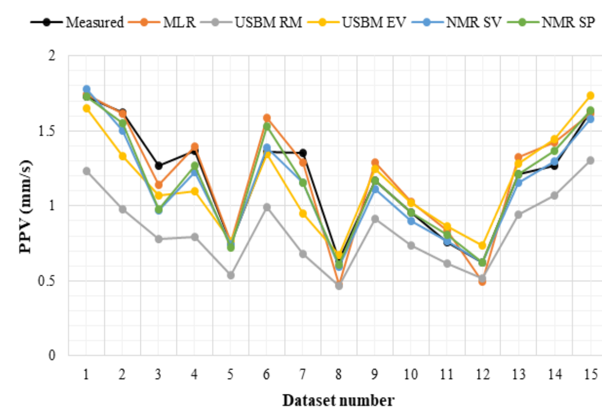

Figure 6. Comparison of measured and predicted PPVs of the testing dataset.

The overall performance of the traditional USBM model with recommended constants is 20% on both regression and testing data. With specifically evaluated site constants, the performance of the USBM model increases to 40% for both the regression and testing data. This enhanced performance with estimated constants confirmed that attenuation constants are specific to blast sites and regions [70].

The Excel Solver solution in the blast geometry modified USBM has an overall performance of 88% and 92% on regression and testing data, respectively. The SPSS nonlinear optimization on the same blast geometry modified USBM model produces an overall performance of 96% on the regression data and 88% on the testing data. The results show significant evidence that the prediction of PPV with only scaled distance is of lower accuracy when compared with the incorporation of blast geometry [9]. The results show that weighted calculation can significantly improve the precision of the vibration prediction model, and regression analysis is very suitable for predicting peak particle velocity in blasting. Thus, blast geometry and dimensions are vital in evaluating blast-induced ground vibration.

Figure 7 shows the neuron network of the combined regression and testing data with one hidden layer. Figure 8 displays the neural network's relative and normalized importance of investigated parameters. The predicted values from the neural network regression and the measured PPV values are plotted in Figure 9 with a strong determination coefficient of 0.93. There is significant evidence that all the tested parameters are essential in predicting peak particle velocity. However, scaled distance remains the most important parameter for evaluating blast-induced vibration using the concept of peak particle velocity, as opined by Yan et al. [8] and Faradonbeh and Monjezi [17].

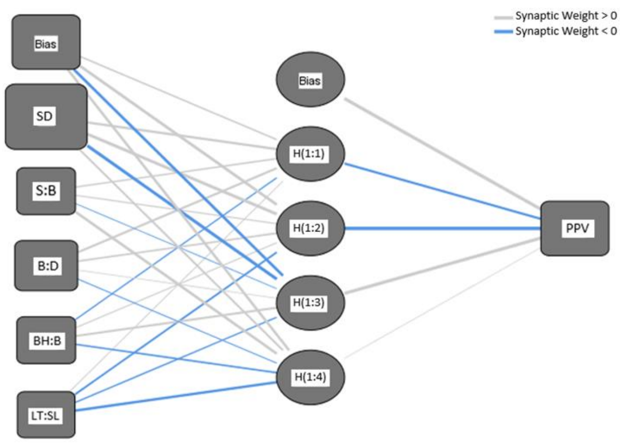

Figure 7. Generated neural network of neurons.

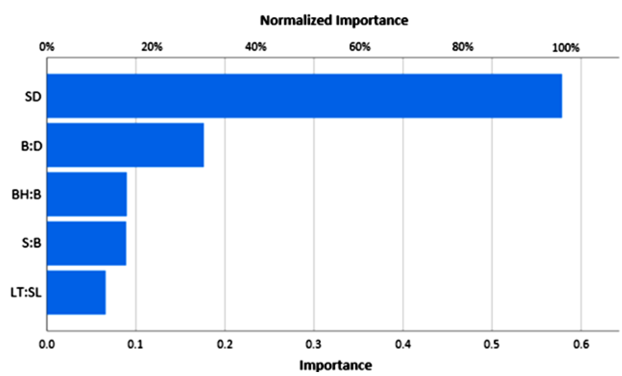

Figure 8. Relative importance of investigated parameters.

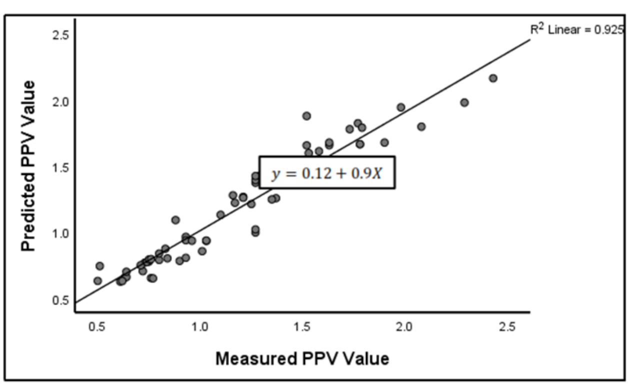

Figure 9. Predicted PPV vs. measured PPV.

7. Conclusion

In this study, the effect of blast geometry on blast-induced ground vibration has been numerically investigated using multiple linear regression, USBM empirical model, and nonlinear multiple regressions. Scaled distance is still the most potent factor in the prediction of blast vibration but yields lower accuracy when used as the only predictor variable. Better and higher prediction accuracy can be obtained if complemented with blast geometry.

The blast geometry modified USBM in a nonlinear multiple regression model iterated in Excel Solver has an overall ranking of 88% and 92% on regression and testing data, respectively. The cumulative grading of the modified USBM iterated in SPSS yielded 96% and 88% on regression and testing data, respectively. Predictions using only scaled distance ranked 20% and 40% on recommended and evaluated site constants for regression and testing data.

Therefore, the incorporation of blast geometry in a modified USBM in Nonlinear multiple regression proved very effective in evaluating blast vibration using the concept of peak particle velocity. The cumulative performance of the investigated parameters using a neural network shows an excellent relationship between peak particle velocity as a dependent variable and scaled distance and blast geometry as predictor variables with a determination coefficient of 0.93. Hence, blast geometry or dimensions are essential in evaluating blast-induced ground vibration.

This work is limited to only two quarries in Bukit Mertajam in Penang, Malaysia. The results of this work can be improved with large data obtained over a long period from many locations. Further study is required by incorporating the effects of the blast pattern into the scaled distance technique of blast-induced ground vibration prediction. The current study only focuses on the blast dimensions (spacing, burden, hole diameter, bench height, stemming length, and total depth).

Acknowledgments

We appreciate the management of FYS Marketing SDN. BHD and Kuad SDN. BHD for granting access to the datasets used for this study.

Conflict of Interest

This manuscript has not been submitted to, nor is it under review at, another journal or other publishing venue. The authors have no affiliation with any organization with a direct or indirect financial interest in the subject matter discussed in the manuscript.

References

[1]. Dhekne PY. Environmental Impacts of Rock Blasting and Their Mitigation. Int J Chem Environ Biol Sci 2015;3:46–50.

[2]. Fattahi H, Ghaedi H. Optimizing Mining Economics: Predicting Blasting Costs in Limestone Mines Using the RES-Based Method. Int J Min Geo-Engineering 2024;58:181–90. https://doi.org/10.22059/IJMGE.2024.363654.595091.

[3]. Bakhtavar E, Abdollahisharif J, Mohammadi D. Analysis and improvement of blasting operation in porphyry, diorite dyke, and trachyte Sungun zones: In-situ investigations. Int J Min Geo-Engineering.2022;56:19–24. https://doi.org/10.22059/ijmge.2021.272288.594772.

[4]. Spathis AT. On the Energy Efficiency of Blasting. 4th Int. Symp. Rock Fragm. by Blasting, Johannesburg: 1999, p. 81–90.

[5]. Konya CJ, Walter EJ. Surface Blast Design. 1st ed. Englewood Cliffs, New Jersey: Prentice Hall; 1990.

[6]. Singh TN, Singh V. An intelligent approach to prediction and control ground vibration in mines. Geotech Geol Eng 2005. https://doi.org/10.1007/s10706-004-7068-x.

[7]. Kuzu C, Ergin H. An assessment of environmental impacts of quarry-blasting operation: A case study in Istanbul, Turkey. Environ Geol 2005. https://doi.org/10.1007/s00254-005-1291-5.

[8]. Yan Y, Hou X, Fei H. Review of predicting the blast-induced ground vibrations to reduce impacts on ambient urban communities. J Clean Prod 2020;260. https://doi.org/10.1016/j.jclepro.2020.121135.

[9]. Blair DP. Blast vibration dependence on charge length, velocity of detonation and layered media. Int J Rock Mech Min Sci 2014;65:29–39. https://doi.org/https://doi.org/10.1016/j.ijrmms.2013.11.007.

[10]. Arthur CK, Bhatawdekar RM, Mohamad ET, Sabri MMS, Bohra M, Khandelwal M, et al. Prediction of Blast-Induced Ground Vibration at a Limestone Quarry: An Artificial Intelligence Approach. Appl Sci 2022;12.

https://doi.org/10.3390/app12189189.

[11]. Iramina WS, Sansone EC, Wichers M, Wahyudi S, Eston SM de, Shimada H, et al. Comparing blast-induced ground vibration models using ANN and empirical geomechanical relationships. REM - Int Eng J 2018;71:89–95.

[12]. Meng Q, Xue H, Song H, Zhuang X, Rabczuk T. Rigid-Block DEM Modeling of Mesoscale Fracture Behavior of Concrete with Random Aggregates. J Eng Mech 2023;149. https://doi.org/10.1061/JENMDT.EMENG-6784.

[13]. Afrasiabian B, Ahangari K, Noorzad A. Study on the effects of blast damage factor and blast design parameters on the ground vibration using 3D discrete element method. Innov Infrastruct Solut 2020;5:37. https://doi.org/10.1007/s41062-020-0286-0.

[14]. Behzadafshar K, Mohebbi F, Soltani Tehrani M, Hasanipanah M, Tabrizi O. Predicting the ground vibration induced by mine blasting using imperialist competitive algorithm. Eng Comput (Swansea, Wales) 2018;35:1774–87. https://doi.org/10.1108/EC-08-2017-0290.

[15]. Cevizci H. The environmental and ecological effects of the plaster stemming method for blasting: A case study . Ekoloji 2015;24:17–22. https://doi.org/10.5053/ekoloji.2015.11.

[16]. Dindarloo SR. Peak particle velocity prediction using support vector machines: a surface blasting case study. J South African Inst Min Metall 2015;115:637–43.

[17]. Faradonbeh RS, Monjezi M. Prediction and minimization of blast-induced ground vibration using two robust meta-heuristic algorithms. Eng Comput 2017;33:835–51. https://doi.org/10.1007/s00366-017-0501-6.

[18]. Koçaslan A, Yüksek AG, Görgülü K, Arpaz E. Evaluation of blast-induced ground vibrations in open-pit mines by using adaptive neuro-fuzzy inference systems. Environ Earth Sci 2017;76. https://doi.org/10.1007/s12665-016-6306-x.

[19]. Mokfi T, Shahnazar A, Bakhshayeshi I, Derakhsh AM, Tabrizi O. Proposing of a new soft computing-based model to predict peak particle velocity induced by blasting. Eng Comput 2018;34:881–8. https://doi.org/10.1007/s00366-018-0578-6.

[20]. Prashanth R, Nimaje DS. Estimation of ambiguous blast-induced ground vibration using intelligent models: A case study. Noise Vib Worldw 2018;49:147–57. https://doi.org/10.1177/0957456518781858.

[21]. Prashanth R, Nimaje DS. Estimation of peak particle velocity using soft computing technique approaches: a review. Noise Vib Worldw 2018;49:302–10. https://doi.org/10.1177/0957456518799536.

[22]. Shirani Faradonbeh R, Jahed Armaghani D, Abd Majid MZ, MD Tahir M, Ramesh Murlidhar B, Monjezi M, et al. Prediction of ground vibration due to quarry blasting based on gene expression programming: a new model for peak particle velocity prediction. Int J Environ Sci Technol 2016;13:1453–64. https://doi.org/10.1007/s13762-016-0979-2.

[23]. Xue X, Yang X, Li P. Evaluation of Ground Vibration Due to Blasting Using Fuzzy Logic. Geotech Geol Eng 2017;35:1231–7. https://doi.org/10.1007/s10706-017-0162-7.

[24]. Yang H, Hasanipanah M, Tahir MM, Bui DT. Intelligent Prediction of Blasting-Induced Ground Vibration Using ANFIS Optimized by GA and PSO. Nat Resour Res 2020;29:739–50. https://doi.org/10.1007/s11053-019-09515-3.

[25]. Garai D, Agrawal H, Mishra AK, Kumar S. Influence of initiation system on blast-induced ground vibration using random forest algorithm, artificial neural network, and scaled distance analysis. Math Model Eng Probl 2018;5:418–26. https://doi.org/https://doi.org/10.18280/mmep.050419.

[26]. Shahrin MI, Abdullah RA, Sa'ari R, Alel MNA, Jeon S, Jeon B. Effect of Burden to Hole Diameter Ratio on Rock Fragmentation by Blasting Using LS-DYNA. In: Aydan Ö, Ito T, Seiki T, Kamemura K, Iwata N, editors. ISRM Rock Dyn. Summit, Okinawa, Japan: CRC Press, Taylor & Francis Group; 2019. https://doi.org/10.1201/9780429327933-112.

[27]. Kou S-Q, Rustan A. Burden related to blasthole diameter in rock blasting. Int J Rock Mech Min Sci Geomech Abstr 1992;29:543–53. https://doi.org/https://doi.org/10.1016/0148-9062(92)91612-9.

[28]. Konya CJ. Blast Design. Ohio 44064, USA: Intercontinental Development Corporation; 1995.

[29]. Hagan T. The Influence of Controllable Blast Parameters on Fragmentation and Mining Costs. In: Rustan A, Holmberg R, editors. 1st Int. Symp. Rock Fragm. by Blasting, Lulea, Sweden: Johnson, Daniel; 1983, p. 31–51.

[30]. Prasad S, Choudhary BSS, Mishra AKK. Effect of Stemming to Burden Ratio and Powder Factor on Blast Induced Rock Fragmentation – A Case Study. IOP Conf Ser Mater Sci Eng 2017;225:12191. https://doi.org/10.1088/1757-899X/225/1/012191.

[31]. Ko Y, Shin C, Jeong Y, Cho S. Blast Hole Pressure Measurement and a Full-Scale Blasting Experiment in Hard Rock Quarry Mine Using Shock-Reactive Stemming Materials. Appl Sci 2022;12. https://doi.org/10.3390/app12178629.

[32]. Sazid M, Singh TN. Numerical assessment of spacing–burden ratio to effective utilization of explosive energy. Int J Min Sci Technol 2015;25:291–7. https://doi.org/https://doi.org/10.1016/j.ijmst.2015.02.019.

[33]. Gao Q, Lu W, Leng Z, Yang Z, Zhang Y, Hu H. Effect of Initiation Location within Blasthole on Blast Vibration Field and Its Mechanism. Shock Vib 2019;2019:1–18. https://doi.org/https://doi.org/10.1155/2019/5386014.

[34]. Leng Z, Fan Y, Gao Q, Hu Y. Evaluation and optimization of blasting approaches to reducing oversize boulders and toes in open-pit mine. Int J Min Sci Technol 2020;30:373–80. https://doi.org/https://doi.org/10.1016/j.ijmst.2020.03.010.

[35]. Minchinton A. On the Influence of Fundamental Detonics on Blasting Practice. In: Spathis AT, Gribble DP, Torrance AC, Little TN, editors. 11th Int. Symp. Rock Fragm. by Blasting (FRAGBLAST 11), Sydney, NSW, Australia: Australasian Institute of Mining and Metallurgy; 2015, p. 41–53.

[36]. Rouse NT. The relative effect of charge dimensions on elastic vibration attenuation and blast-induced seismic energy concepts. Missouri University of Science and Technology, 2015.

[37]. Himanshu VK, Roy MP, Mishra AK, Paswan RK, Panda D, Singh PK. Multivariate statistical analysis approach for prediction of blast-induced ground vibration. Arab J Geosci 2018;11. https://doi.org/10.1007/s12517-018-3796-8.

[38]. Himanshu VK, Roy MP, Mishra AK, Mishra R, Singh PK. Dynamic simulation approach to assess influence of charging parameters on blast induced vibration. J Mines, Met Fuels 2019;67:299–306.

[39]. Singh SP, Abdul H. Investigation of blast design parameters to optimize fragmentation. In: Singh PK, Sinha A, editors. 10th Int. Symp. Rock Frag- mentation by Blasting (FRAGBLAST 10), New Delhi, India: Taylor & Francis Group, London; 2012, p. 181–5.

[40]. Uysal Ö, Arpaz E, Berber M. Studies on the effect of burden width on blast-induced vibration in open-pit mines. Environ Geol 2007;53:643–50. https://doi.org/10.1007/s00254-007-0679-9.

[41]. Rezaeineshat A, Monjezi M, Mehrdanesh A, Khandelwal M. Optimization of blasting design in open pit limestone mines with the aim of reducing ground vibration using robust

techniques. Geomech Geophys Geo-Energy Geo-Resources 2020;6. https://doi.org/10.1007/s40948-020-00164-y.

[42]. Singh PK, Roy MP, Paswan RK, Sarim M, Kumar S, Jha RR. Rock fragmentation control in opencast blasting. J Rock Mech Geotech Eng 2016;8:225–37. https://doi.org/10.1016/j.jrmge.2015.10.005.

[43]. Arthur CK, Kaunda RB. A hybrid paretosearch algorithm and goal attainment method for maximizing production and reducing blast-induced ground vibration: a blast design parameter selection approach. Min Technol Trans Inst Min Metall 2020:1–8. https://doi.org/10.1080/25726668.2020.1790262.

[44]. Jahed Armaghani D, Kumar D, Samui P, Hasanipanah M, Roy B. A novel approach for forecasting of ground vibrations resulting from blasting: modified particle swarm optimization coupled extreme learning machine. Eng Comput 2020. https://doi.org/10.1007/s00366-020-00997-x.

[45]. Abd. Rahman AH, Ibrahim MZ, Ramachandram Y V. Coastal Sedimentation and Recent Coastline Changes Along the Seberang Perai Coast, Pulau Pinang. Geol. Soc. Malaysia Annu. Geol. Conf., Penang, Malaysia: Geological Society of Malaysia; 2000, p. 169–76.

[46]. Ghani AA, Doya BM, Teh GH. Age, petrochemistry and modelling of the Bukit Mertajam-Kulim granite, northwest Peninsular Malaysia. Bull Geol Soc Malaysia 2000;44:139–50.

[47]. Lawal AI, Idris MA. An artificial neural network-based mathematical model for the prediction of blast-induced ground vibrations. Int J Environ Stud 2020;77:318–34. https://doi.org/10.1080/00207233.2019.1662186.

[48]. Ragam P, Nimaje DS. Evaluation and prediction of blast-induced peak particle velocity using artificial neural network: A case study. Noise Vib Worldw 2018;49:111–9. https://doi.org/10.1177/0957456518763161.

[49]. Yilmaz O. The comparison of most widely used ground vibration predictor equations and suggestions for the new attenuation formulas. Environ Earth Sci 2016;75:1–11. https://doi.org/10.1007/s12665-015-5011-5.

[50]. Abedi AS, Hataf N, Shivaei S, Ghahramani A. Comparative study of analytical and numerical evaluation of the dynamic response of buried pipelines to road-cut excavation blasting. Geomech Geoengin 2020;15:140–8. https://doi.org/10.1080/17486025.2019.1634289.

[51]. Adepitan RO, Owolabi A, Komolafe K. Prediction of structural response to blast –induced vibration in Kopek Construction Quarry, Ikere–Ekiti, Ekiti State, Nigeria. Int J Environ Stud 2018;75:990–9. https://doi.org/10.1080/00207233.2018.1473207.

[52]. Cihangir F. Cautious blasting around nearby buildings. Int. Multidiscip. Sci. GeoConference Surv. Geol. Min. Ecol. Manag. SGEM, vol. 18, Department of Mining Eng, Karadeniz Technical University, Trabzon, Turkey: 2018, p. 151–8. https://doi.org/10.5593/sgem2018/1.3/S03.020.

[53]. Hasanipanah M, Naderi R, Kashir J, Noorani SA, Zeynali Aaq Qaleh A. Prediction of blast-produced ground vibration using particle swarm optimization. Eng Comput 2017;33:173–9. https://doi.org/10.1007/s00366-016-0462-1.

[54]. Kumar S, Choudhary BS. Prediction of blast-induced ground vibration by ANN, USBM and CMRI formulae for safety of the structures near surface coal mines. J Mines, Met Fuels 2019;67:351–6.

[55]. Duvall WI, Petkof B. Spherical propagation of explosion-generated strain pulses in rock. 1959.

[56]. Fogelson D, Atchison TC, Duvall WI. Propagation of peak strain and strain energy for explosion-generated strain pulses in Rock. Seismol Res Lett 1959;30:34–34. https://doi.org/10.1785/gssrl.30.3.34a.

[57]. Siskind DE, Stagg MS, Kopp JW, Dowding CH. Structure response and damage produced by ground vibration from surface mine blasting. Int J Rock Mech Min Sci Geomech Abstr 1981;18:76. https://doi.org/https://doi.org/10.1016/0148-9062(81)91353-X.

[58]. Standards Australia. AS 2187.2 - 2006: Explosives - Storage, Transport, and Use. Part 2: Use of Explosives. 2006.

[59]. Aloui M, Bleuzen Y, Essefi E, Abbes C. Evaluation of ground vibrations and the effect of air blast in open-pit phosphate mines. Arab J Geosci 2018;11. https://doi.org/10.1007/s12517-018-4025-1.

[60]. Aloui M, Abbes C. Fracturing Influence on the Propagation of the Blast-Induced Ground Vibrations: A Case Study. Geotech Geol Eng 2019;37:5327–39. https://doi.org/10.1007/s10706-019-00982-2.

[61]. Hudaverdi T, Akyildiz O. Investigation of the site-specific character of blast vibration prediction. Environ Earth Sci 2017;76. https://doi.org/10.1007/s12665-017-6456-5.

[62]. Maran Beena A, Pani AK. Fault Detection of Complex Processes Using nonlinear Mean Function Based Gaussian Process Regression: Application to the Tennessee Eastman Process. Arab J Sci Eng 2021;46:6369–90. https://doi.org/10.1007/s13369-020-05052-x.

[63]. Bahaaddini M, Hosseinpour Moghadam E. Evaluation of empirical approaches in estimating the deformation modulus of rock masses. Bull Eng Geol Environ 2019;78:3493–507. https://doi.org/10.1007/s10064-018-1347-x.

[64]. Aladejare AE. Evaluation of empirical estimation of uniaxial compressive strength of rock using measurements from index and physical tests. J Rock Mech Geotech Eng 2020;12:256–68. https://doi.org/10.1016/j.jrmge.2019.08.001.

[65]. Swamidass PM. MAPE (mean absolute percentage error). In: Swamidass PM, editor. Encycl. Prod. Manuf. Manag., Boston, MA: Springer US; 2000, p. 462. https://doi.org/10.1007/1-4020-0612-8_580.

[66]. Hyndman RJ, Koehler AB. Another look at measures of forecast accuracy. Int J Forecast 2006;22:679–88. https://doi.org/https://doi.org/10.1016/j.ijforecast.2006.03.001.

[67]. Willmott CJ, Matsuura K. On the use of dimensioned measures of error to evaluate the performance of spatial interpolators. Int J Geogr Inf Sci 2006;20:89–102. https://doi.org/10.1080/13658810500286976.

[68]. Wyllie DC, Mah CW. Rock Slope Engineering: Civil and Mining. 4th ed. London: CRC Press; 2017. https://doi.org/https://doi.org/10.1201/9781315274980.

[69]. White TJ, Pegden M, Birch WJ. Developments in the use of scaled-distance modelling which allow an increase in the permitted charge weights while still ensuring vibration compliance. In: Holmberg R, editor. 2nd World Conf. Explos. Blasting Tech., Prague, Czech Republic: A.A. Balkema; 2003, p. 89–96.

[70]. Ozer U, Karadogan A, Kahriman A, Aksoy M. Bench blasting design based on site-specific attenuation formula in a quarry. Arab J Geosci 2013;6:711–21. https://doi.org/10.1007/s12517-011-0388-2.